

Supporting information

Tailoring multi-system adaptable gel polymer electrolyte for realization of carbonate ester and ether-based Li-SPAN batteries

Yan Zhang, Zhaokun Wang, Yanrui Pan, Hao Yu, Zuohang Li, Chen Li, Su Wang, Yue Ma*, Xixi Shi, Hongzhou Zhang, Dawei Song and Lianqi Zhang*

Experimental section

Materials

Pentaerythritol tetraacrylate (PETEA, >97.0%) was purchased from Shanghai Macklin Biochemical Co., Ltd. 2,2,3,4,4,4-Hexafluorobutyl Acrylate (HFBA, ≥95.0%) and azobisisobutyronitrile (AIBN, ≥99%) were purchased from Sigma-Aldrich Inc. PETEA, HFBA and AIBN were stored at 2-8 °C. The commercial liquid electrolytes (1.0 M LiTFSI in DOL: DME = 1: 1 vol% with 1 wt.% LiNO₃ and 1.0 M LiPF₆ in EC: DMC = 1: 1 vol% with 1 wt.% FEC) were purchased from Suzhou DoDoChem Technology Co., Ltd. Lithium foil was purchased from China Energy Lithium Co., Ltd. Sublimed sulfur was purchased from Tianjin Kewei Co., Ltd. Polyacrylonitrile (PAN, Mw = 150,000) was purchased from Shanghai Macklin Biochemical Co., Ltd. N-methyl-2-pyrrolidone (NMP), poly(vinylidene fluoride) (PVDF) and acetylene black was purchased from Sigma-Aldrich Inc. All reagents were used as received without any further purification.

Cathode Preparation

Sulfurized polyacrylonitrile (SPAN) was self-prepared according to a previously reported procedure with a slight amendment. Briefly, the sample was prepared by mixing sublimed sulfur with PAN in 4:1 weight ratio using a mortar and pestle. The mixing sample was placed in a quartz tube at 450 °C for 6h with 5 °C min⁻¹ heating ramping under a constant nitrogen flow (200 L h⁻¹). Then, the tube was heated to 155 °C to remove unresponsive sulfur. The SPAN was washed with toluene using Soxhlet extraction for 48h to remove excess sulfur. Finally, the SPAN composite was dried under vacuum at 60 °C for further utilization. The cathodes were prepared by casting homogeneous slurry containing SPAN composite (70 wt.%), acetylene black (20 wt.%), and PVDF binder (10 wt.%) on Al foil. Then drying at 55 °C for 24h, the cathode was punched into φ 12 mm laminate with an areal density of 0.63 mg cm⁻².

Preparation of in-situ gel polymer electrolyte (PFGPE)

To prepare the PFGPE by in-situ polymerization, polymer monomers were contained in a liquid electrolyte (LE). Typically, HFBA monomer and PETEA crosslinker were co-dissolved in LE consisting of 1.0 M lithium bis(trifluoromethane sulfonyl)imide (LiTFSI) salt in a mixture of 1,3-dioxolane (DOL)/dimethoxymethane (DME) (1: 1 vol%) with 1 wt.% LiNO₃ in the weight ratio of 1: 1. According to the same method, ester-based PFGPE was prepared, only ether-based liquid electrolyte (1.0 M LiTFSI in DOL: DME = 1: 1 vol% with a 1 wt.% LiNO₃) was replaced by ester-based liquid electrolyte (1.0 M LiPF₆ in EC: DMC = 1: 1 vol% with a 1 wt.% FEC). After that, the mixture was stirred for 30 minutes at 25 °C to form a precursor solution. Ultimately, 0.1 wt.% AIBN was added as the thermal initiator for free-radical polymerization. The precursor solution was further initiated by a vacuum oven at 70 °C. The crosslinked polymer electrolyte PFGPE with a solid content of 3 wt.% was obtained after polymerization for 4h. All experiments were conducted under the dry argon atmosphere. The polymer matrix of ether-based PFGPE was isolated and clarified for further characterization as follows: the monomers were dissolved in the solvent of DOL: DME (1: 1 vol%) to obtain the wet gels. Subsequently, the mixture was washed with DME three times to remove the impurities. Finally, the separated polymer was obtained after vacuum drying at 60 °C.

Preparation of the battery

The cathode was punched into disks 12 mm in diameter with an areal density of 0.6-0.7 mg cm⁻². Commercial Cu foil was cut into round Cu chips (ϕ 14 mm), dried in vacuum at 60 °C for 12h. The Celgard 2400 polypropylene (PP) was pre-cut into disks with a diameter of 16.5 mm, and dried under vacuum before use. The CR2032 coin battery is assembled in an Ar-filled glove box using PP as supporting structure to prevent short circuits during the in-situ polymerization. 80 μ L precursor solution containing 1.5 wt.% HFBA, 1.5 wt.% PETEA, and 0.1 wt.% AIBN was dissolved in LE injected in the separator and injected into the batteries. After assembly, the batteries undergo aging for 2h at room temperature to ensure proper wetting of the precursor solution. Then, the as-prepared batteries were placed on the heating stage at 70 °C for 4h to ensure that the in-situ copolymerization crosslinker of HFBA monomer and PETEA was used to obtain PFGPE batteries.

Physical characterization of PFGPE

The cross-linked structure of PFGPE molecular chains was investigated by Fourier transform infrared spectroscopy (FT-IR, Frontier Mid-IR FTIR). The solid-state magic-angle-spinning (MAS) ¹³C NMR measurements of the PFGPE membrane were analyzed using an AVANCE III 400 MHz spectrometer with a 4 mm probe under MAS conditions. The thermal stability of HFBA, PETEA, PFGPE, and LE was investigated using thermogravimetric analyzer (TGA, Netzsch, TG 209 F3 Tarsus) in the range of room temperature ~ 600 °C with a heating rate of 10 °C min⁻¹. The glass transition temperature (T_g) of PFGPE was confirmed by differential scanning calorimetry (DSC, DSC200F3A01). Small-angle X-ray scattering (SAXS, SAXSpace) was used to confirm PFGPE morphology. The cross-section and morphology of PFGPE during cycling were observed by scanning electron microscopy (SEM, Quanta FEG 250). Transmission electron microscopy (TEM, JEM2100PLUS) was applied to characterize the cathode electrolyte interface (CEI). The composition of CEI and solid electrolyte interface (SEI) was tested using X-ray photoelectron spectroscopy (XPS, Thermo Escalab 250). The adsorption properties between PFGPE and LiPS solutions were determined by UV-visible spectrophotometry (the molar ratio of S to Li₂S was 5:1 and the solvent was a mixture of DME/ DOL (1: 1 vol%).

Changes in morphology of Li electrode during the electrochemical deposition process and SPAN during the first discharge process are directly observed by in-situ optical microscope (Beijing Scistar Technology Co., Ltd.). The battery for the microscopy observation was prepared by stacking a Li sheet or a SPAN, an electrolyte solution (1.0 M LiTFSI in DOL: DME = 1: 1 vol% with a 1 wt.% LiNO₃), soaked polypropylene separator (19 mm in diameter, Celgard), and a Li sheet. The positive effect of PFGPE was explored by polymerizing PFGPE on the surface of the electrodes. Then, the battery was placed in a jig for light microscopy and the cross-section of the surface was monitored via an observation window made of sapphire using light microscopy. The electrochemical measurements of Li//Li batteries were performed using the LAND testing system (Wuhan LAND electronics Co., Ltd.) and Neware battery test system (CT-4008T-5V10mA-164, Shenzhen, China) at a constant current of 0.4mA (0.4/cm²) at room temperature and the Li-SPAN batteries were tested at 0.5C.

Electrochemical characterization of PFGPE

The ionic conductivity (σ) of PFGPE was evaluated using electrochemical impedance spectroscopy (EIS) via the PARSTAT MC electrochemical workstation in the frequency range from 1 MHz to 0.1 Hz. The value of σ can be calculated through the following equation (1):

$$\sigma = \frac{d}{RS} \dots \dots \dots (1)$$

where d represents the thickness, and S stands for the area of PFGPE, respectively. R is the bulk resistance of PFGPE originating from the EIS on symmetric stainless steel (SS) batteries. Moreover, the activation energy (E_a) of FGPE was calculated via Vogel-Tamman-Fulcher (VTF) equatio:

$$\sigma = \sigma_0 T^{-\frac{1}{2}} \exp\left(-\frac{E_a}{R(T - T_0)}\right) \dots \dots \dots (2)$$

where σ is the ionic conductivity of FGPE at the temperature range from 30 to 120 °C, σ_0 is pre-exponential factor, E_a belongs to the activation energy, T_0 represents the effective glass transition temperature, and R displays the ideal gas constant. t_{Li^+} of the PFGPE and LE can be measured by direct current (DC) polarization and alternating current (AC) impedance in symmetric Li//Li batteries. The value of t_{Li^+} can be calculated according to the following equation (2):

$$t_{Li^+} = \frac{I_s(\Delta V - I_0 R_0)}{I_0(\Delta V - I_s R_s)} \dots \dots \dots (3)$$

where ΔV (10 mV) is the polarization voltage applied, respectively. While, I_0 and R_0 are the initial current and electrolyte/electrode interfacial resistance, I_s and R_s are the steady-state polarization current and interfacial resistance obtained by EIS after the measure of CA. The electronic conductivity of PFGPE and LE were calculated through the equation:

$$\gamma = \frac{I_s \times l}{S \times U} \dots \dots \dots (4)$$

where l and S are the thickness and surficial area of electrolyte. The surficial area of electrolyte, I_s , and U (1 V) represents the steady state current resulting and the applied potential.

The linear sweep voltammetry (LSV) measurements were conducted using Li as a working electrode and stainless steel laminate as a reference and counter electrode. The CV measurements were conducted in the Princeton electrochemical workstation in the voltage range from 1-3 V at a scan rate of 1mV s⁻¹. The compatibility of electrolytes with Li metal was investigated by galvanostatic cycling/rate method using symmetrical Li//Li battery. The Coulombic efficiencies of Li depositing/stripping in different electrolytes were investigated using Cu//Li half battery at 0.5 mA cm⁻². While the lithium nucleation over potential was investigated by chronopotentiometry measurement using Cu//Li half battery. The cycling and rate performances of batteries at different temperature were carried out on the LAND testing system (Wuhan LAND electronics Co., Ltd.) and Neware battery test system (CT-4008T-5V10mA-164, Shenzhen, China), respectively.

All the DFT calculations were conducted based on the Vienna Ab-initio Simulation Package (VASP)^[1,2]. The exchange-correlation effects were described by the Perdew-Burke-Ernzerhof (PBE) functional

within the generalized gradient approximation (GGA) method [3,4]. The core-valence interactions were accounted by the projected augmented wave (PAW) method [5]. The energy cutoff for plane wave expansions was set to 450 eV. The structural optimization was completed for energy and force convergence set at 1.0×10^{-6} eV and 0.02 eV \AA^{-1} , respectively. The Brillouin zone was sampled with a $3 \times 3 \times 3$ grid centered at the gamma (Γ) point. The cohesive energies of polysulfides are calculated by

$$\Delta E_{CE} = E(S + Li_2S_n) - [E(S) + E(Li_2S_n)] (n = 2,4,6,8) \dots \dots \dots (5)$$

where $E(S)$ represents electronic energies of DOL+DME or PFGPE, $E(Li_2S_n)$ represents the electronic energies of Li_2S_n , and $E(S+Li_2S_n)$ represents the electronic energies of the polysulfide molecule with DOL+DME or PFGPE molecule.

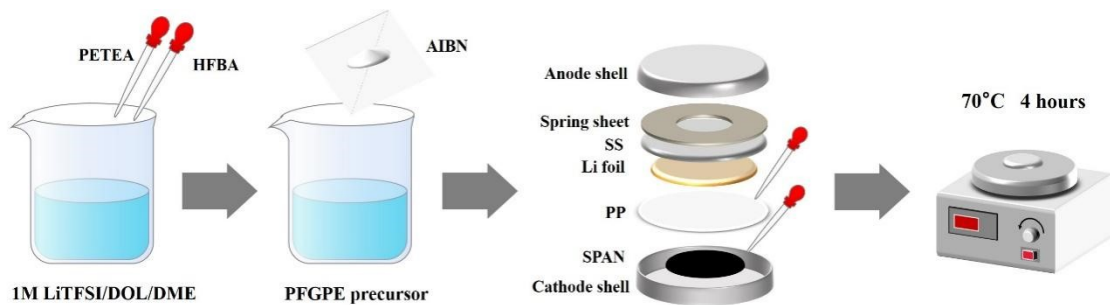


Figure S1. Schematic diagram for the preparation process of PFGPE.

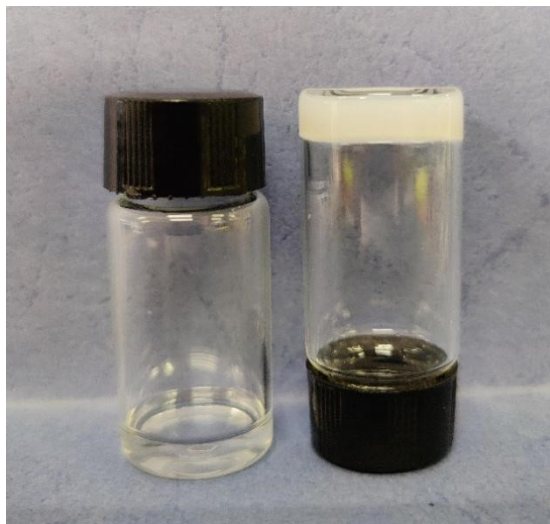


Figure S2. Optical image of polymerization of HFBA, PETEA to form PFGPE.

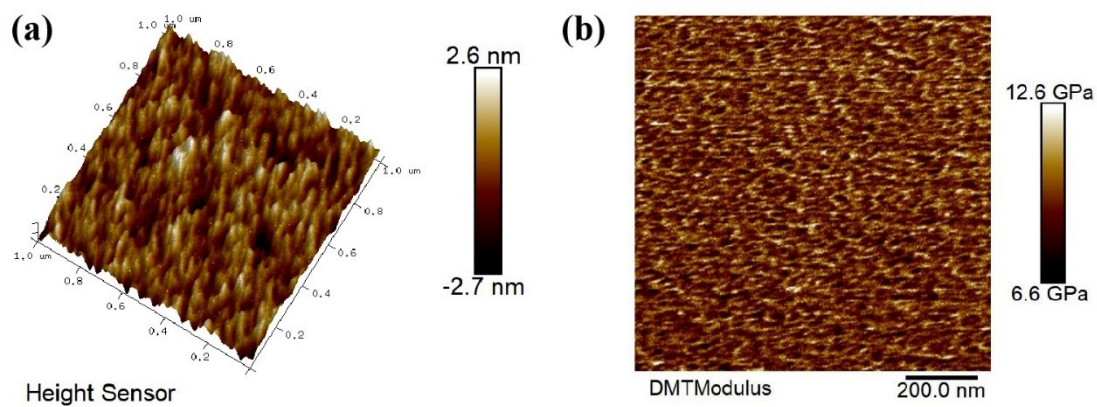


Figure S3. (a) AFM image and (b) Young's modulus mapping of PFGPE.

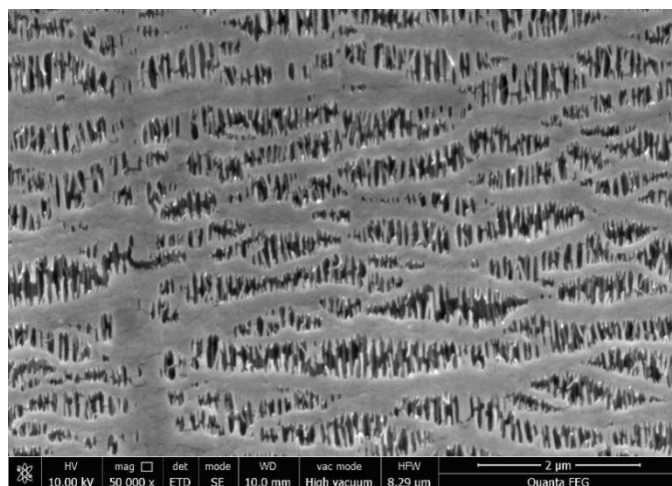


Figure S4. Typical SEM image of Celgard 2400 polypropylene (PP).

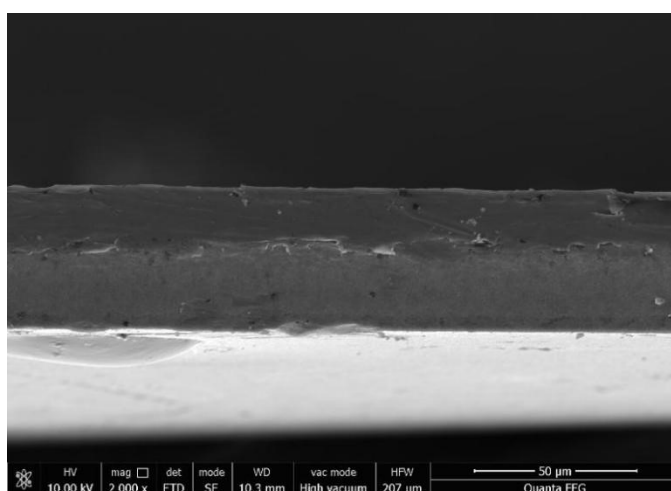


Figure S5. Cross-section of PFGPE polymerized on PP.

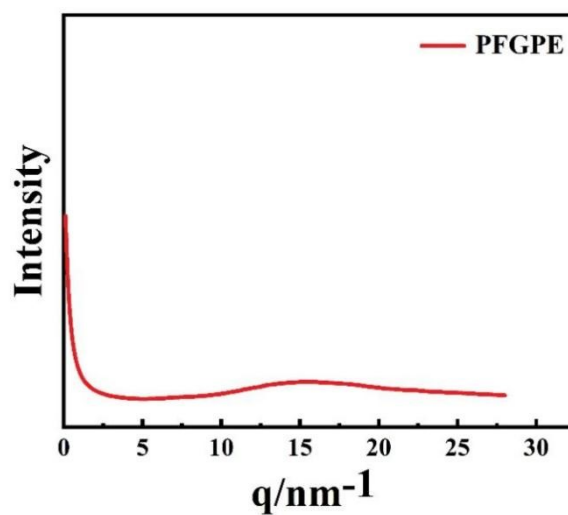


Figure S6. SAXS spectrum of PFGPE.

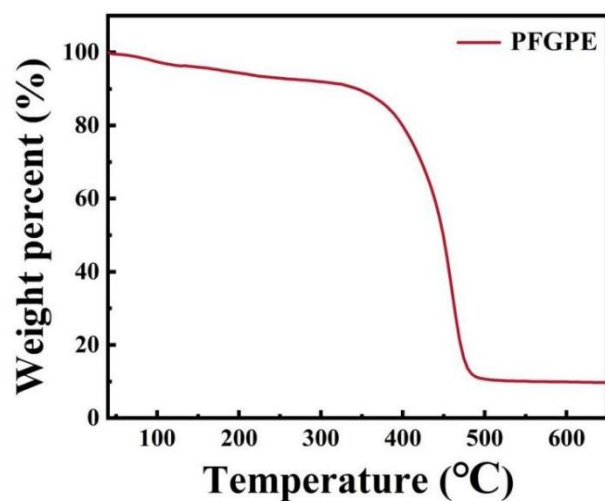


Figure S7. TG profile of PFGPE.

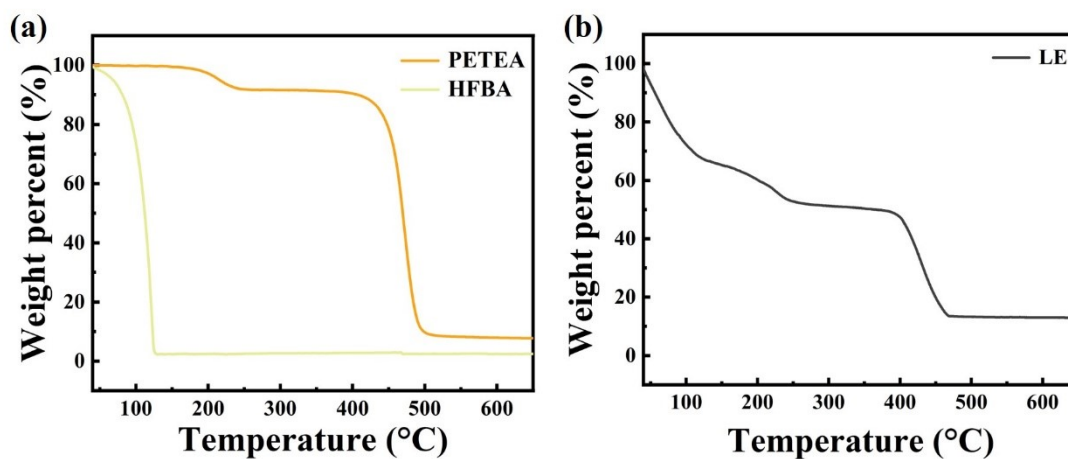


Figure S8. TG comparison of (a) PETEA, HFBA and (b) LE from 40 to 650 °C.

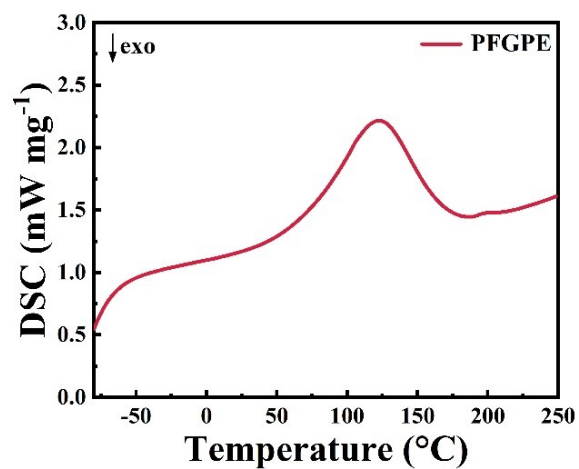


Figure S9. DSC profile of matrix in PFGPE.

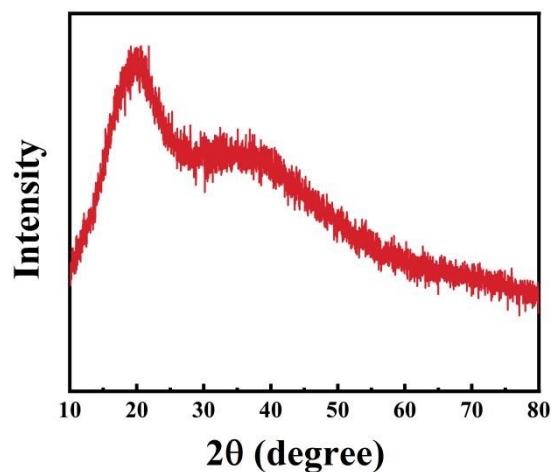


Figure S10. XRD pattern of polymer matrix in PFGPE.

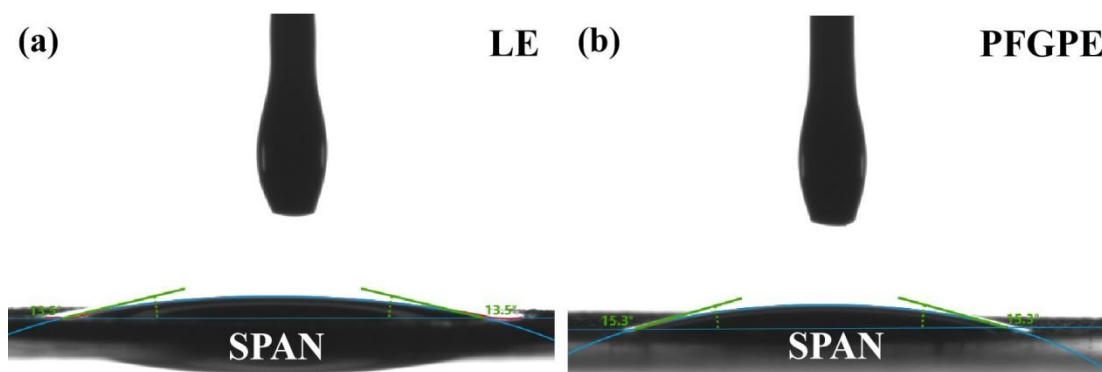


Figure S11. Contact angle of (a) LE/SPAN and (b) PFGPE/SPAN.

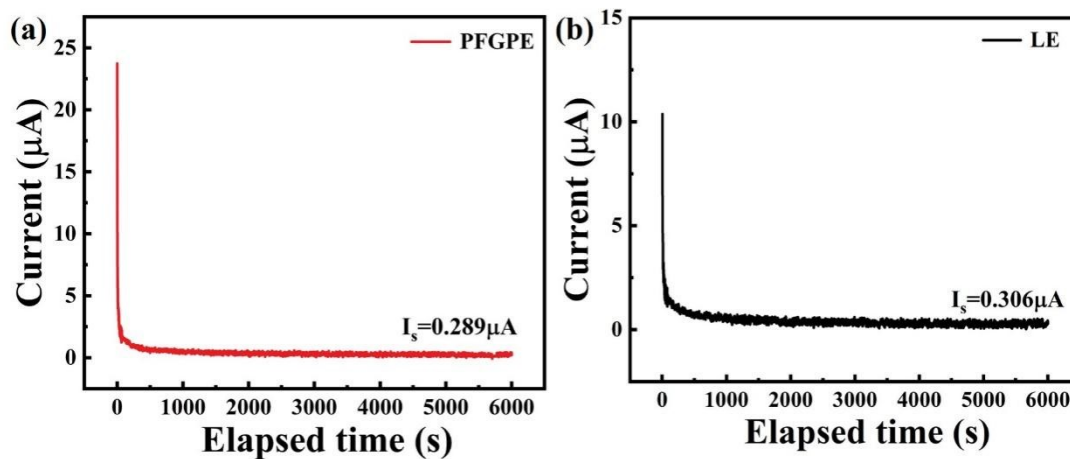


Figure S12. The DC polarization profile of ether-based (a) SS/PFGPE/SS and (b) SS/LE/SS batteries at a constant voltage of 1 V. The electronic conductivity values for PFGPE and LE are calculated to be $9.39 \times 10^{-10} \text{ S cm}^{-1}$ and $6.12 \times 10^{-10} \text{ S cm}^{-1}$, respectively.

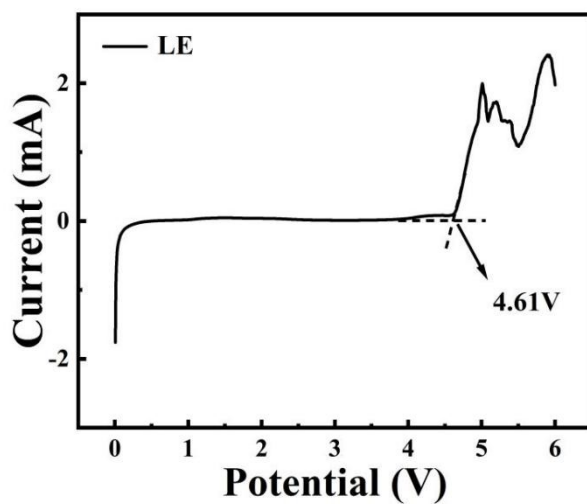


Figure S13. LSV profile of ether-based SS/LE/SS battery.

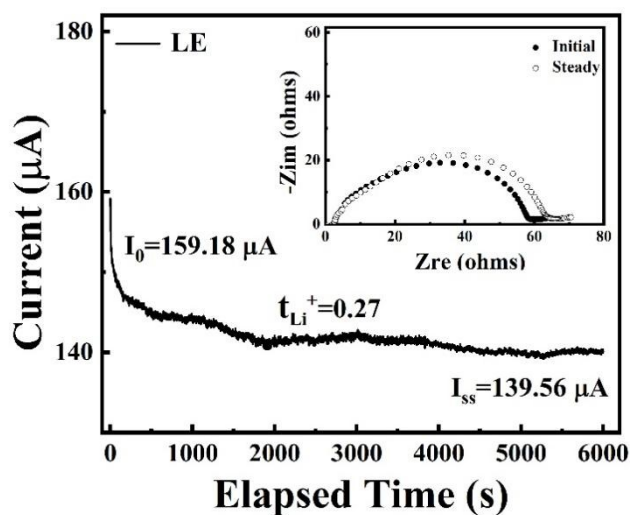


Figure S14. Current-time profile following a DC polarization of 10 mV for ether-based Li/LE/Li symmetrical battery, the insert displays the Nyquist profiles of electrochemical impedance spectroscopy before and after polarization.

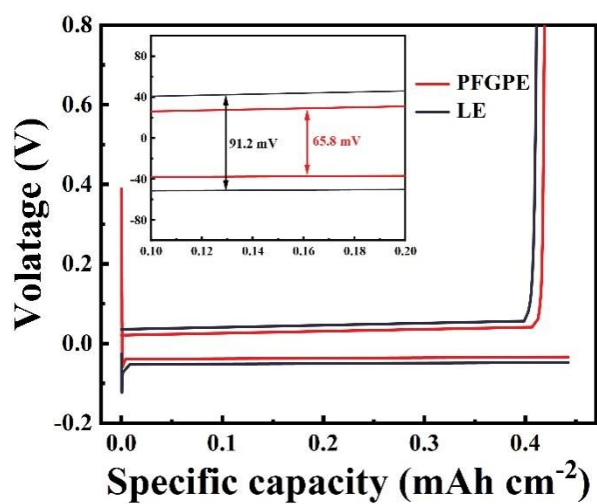


Figure S15. Li stripping/plating curves of ether-based Cu/PFGPE/Li and Cu/LE/Li half batteries at 0.5 mA cm⁻².

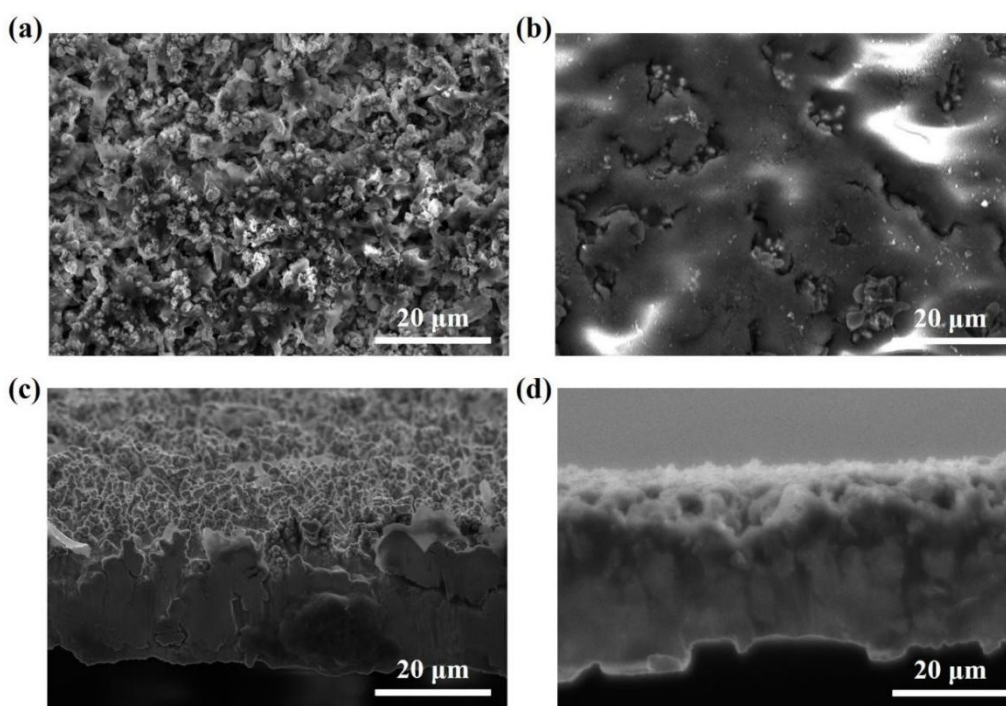


Figure S16. The deposited Li morphology of Cu foil in ether-based (a) Cu/LE/Li and (b) Cu/PFGPE/Li half batteries at 0.5 mA cm⁻². Cross-section Cu foils in cycled (c) Li/LE/Li and (d) Li/PFGPE/Li symmetric batteries.

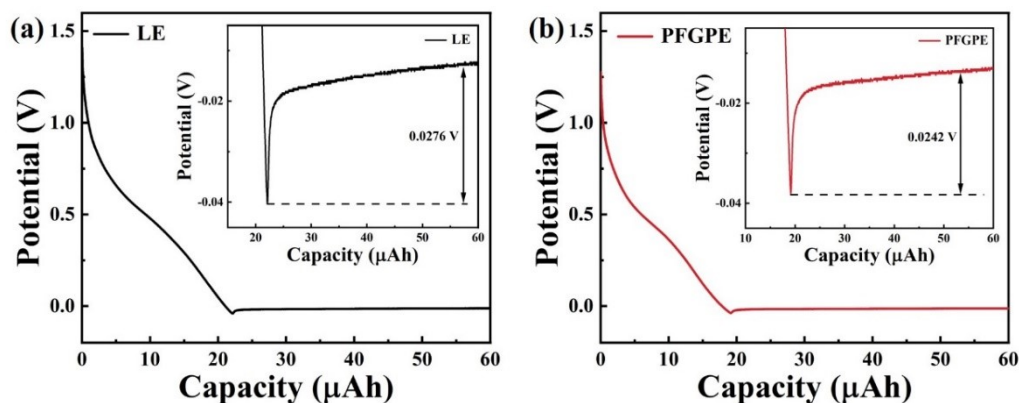


Figure S17. Chronoamperometric comparison of ether-based Cu/PFGPE/Li and Cu/LE/Li half batteries at 0.05 mA cm^{-2} .

The plum-bud potential of different electrolytes was determined by the time potentiometric method. The voltage-capacity profiles voltage dips at the beginning of Li nucleation and then stabilizes [6]. The difference between the bottom of the voltage drop and the flat portion of the voltage platform represents the overpotential for lithium nucleation, which indicates how strongly the collector surface attracts lithium. The Cu/PFGPE interface nuclear energy barrier is lower, compared with ether-based Cu/PFGPE/Li battery (0.0242 mV) and Cu/LE/Li battery (0.0276 mV). PFGPE can effectively inhibit dendrite formation and increase the size of lithium nucleus. However, this difference is not statistically significant due to the low solid content of only 3 wt.% in PFGPE, which is consistent with the results of constant current polarization. In addition, the plateau region is mainly affected by the current density and lithium ion migration characteristics in the electrolyte solution. The lithium core of ether-based Cu/PFGPE/Li batteries is easier to grow. Improved nucleophilicity and reduced mass transfer potential promote enhanced lithium ion deposition dissolution in Cu/PFGPE/Li batteries [7].

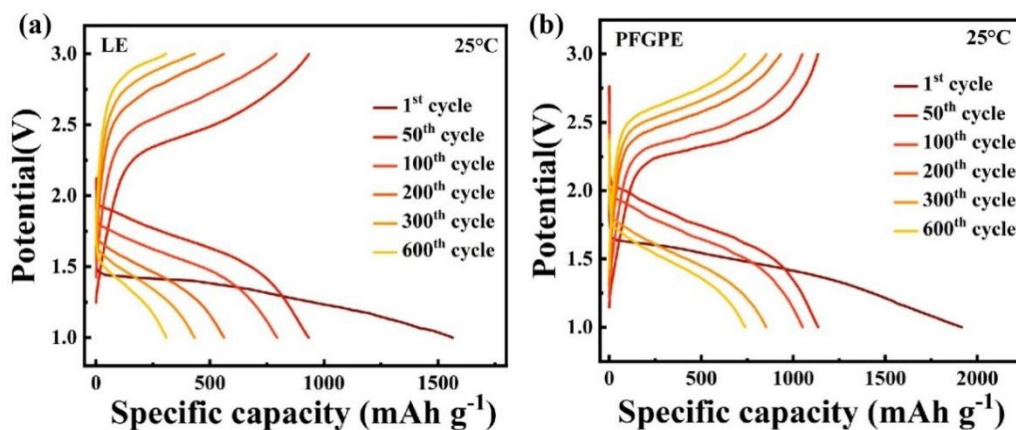


Figure S18. Galvanostatic charge/discharge profiles of ether-based (a) SPAN/LE/Li and (b) SPAN/PFGPE/Li batteries at 0.2C and 25 °C.

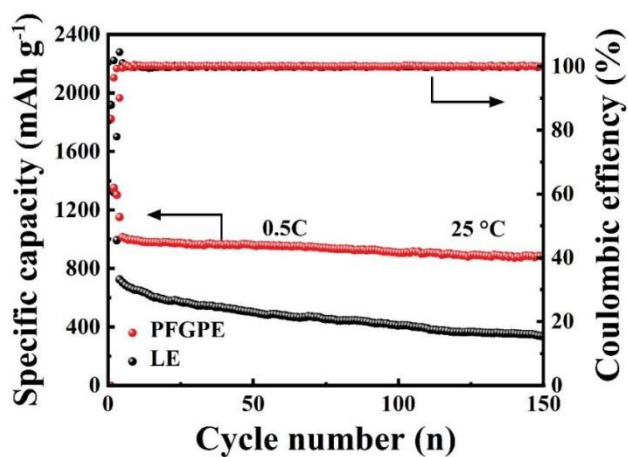


Figure S19. Cycling performances of ether-based SPAN/PFGPE/Li and SPAN/LE/Li batteries at 0.5C and 25 °C.

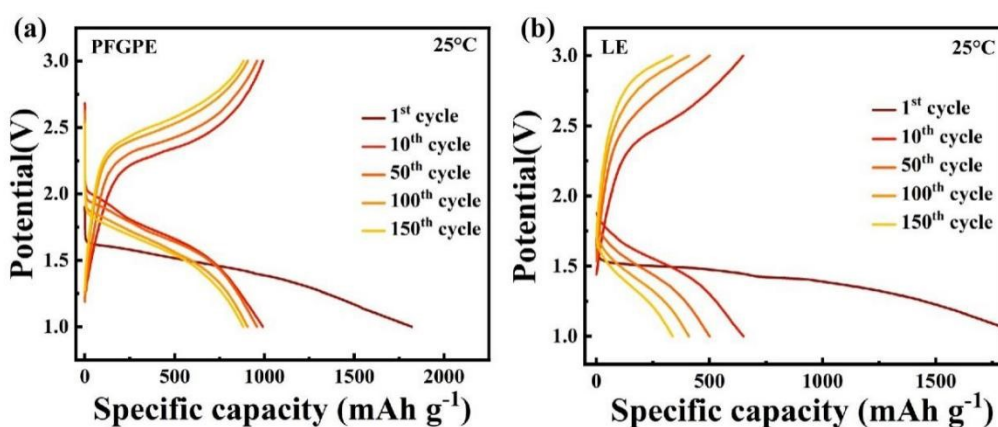


Figure S20. Galvanostatic charge/discharge profiles of ether-based (a) SPAN/PFGPE/Li and (b) SPAN/LE/Li batteries at 0.5C and 25 °C.

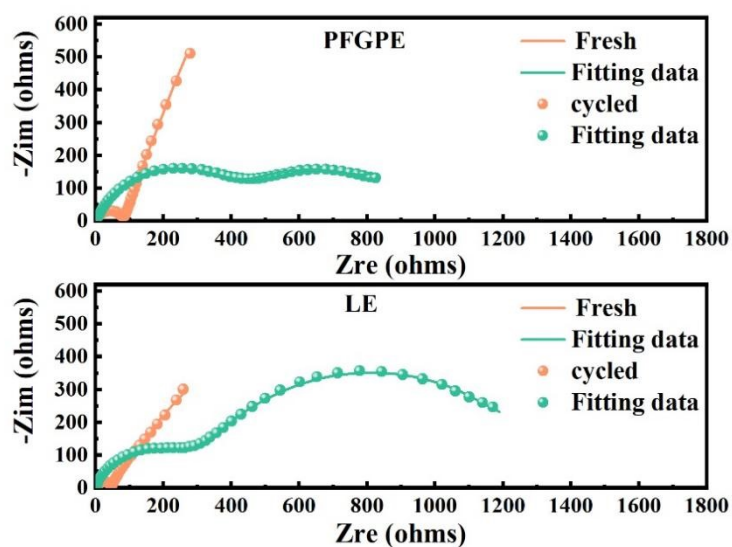


Figure S21. Electrochemical impedance spectra profiles of ether-based SPAN/PFGPE/Li and SPAN/LE/Li batteries at 0.5C and 25 °C.

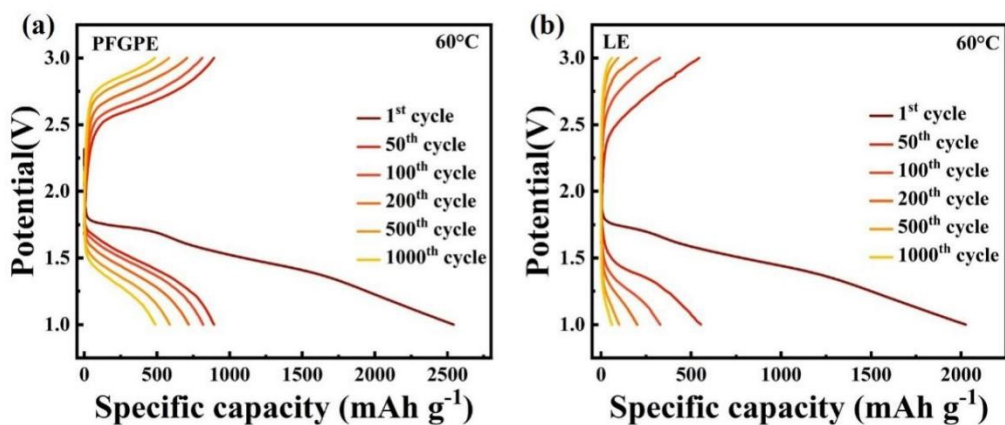


Figure S22. Galvanostatic charge/discharge profiles of ether-based (a)SPAN/PFGPE/Li and (b) SPAN/LE/Li batteries at 0.5C and 60 °C.

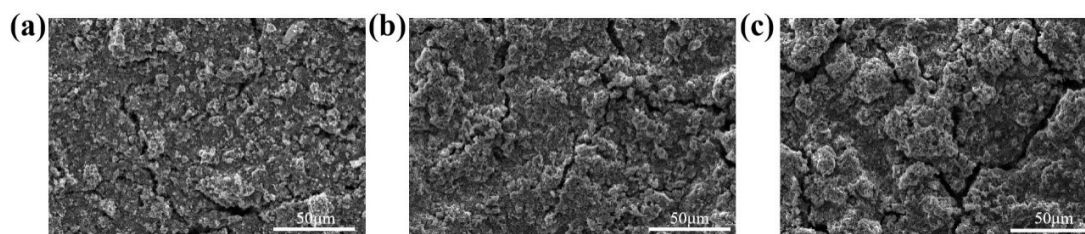


Figure S23. SEM images of (a) pristine and cycled cathode in ether-based (b) SPAN/PFGPE/Li and (c) SPAN/LE/Li batteries after 200 cycles at 0.2C.

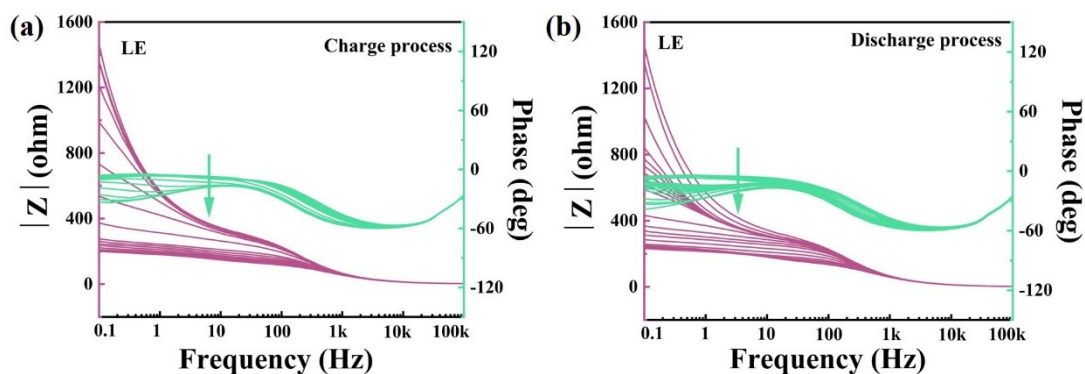


Figure S24. Corresponding bode plots of impedance spectra of ether-based SPAN/LE/Li battery in (a) charge process and (b) discharge process.

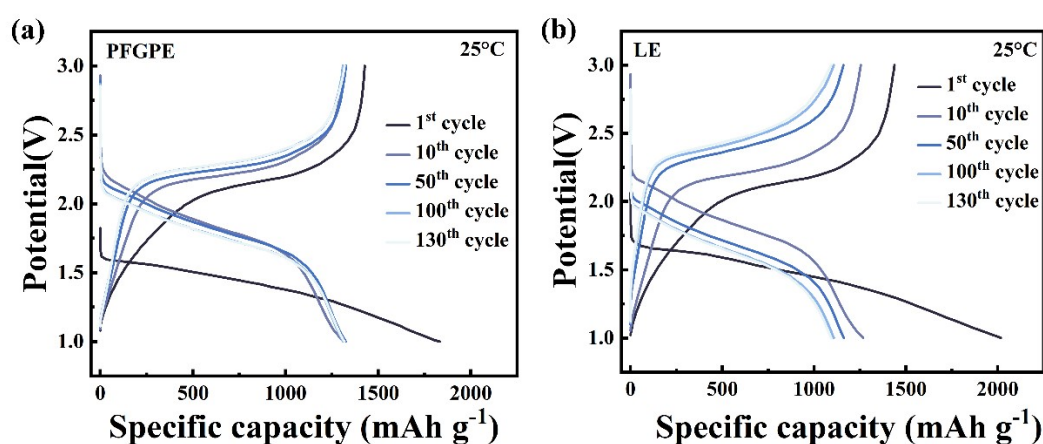


Figure S25. Galvanostatic charge/discharge profiles of ester-based (a) SPAN/PFGPE/Li and (b) SPAN/LE/Li batteries at 0.1C and 25 °C.

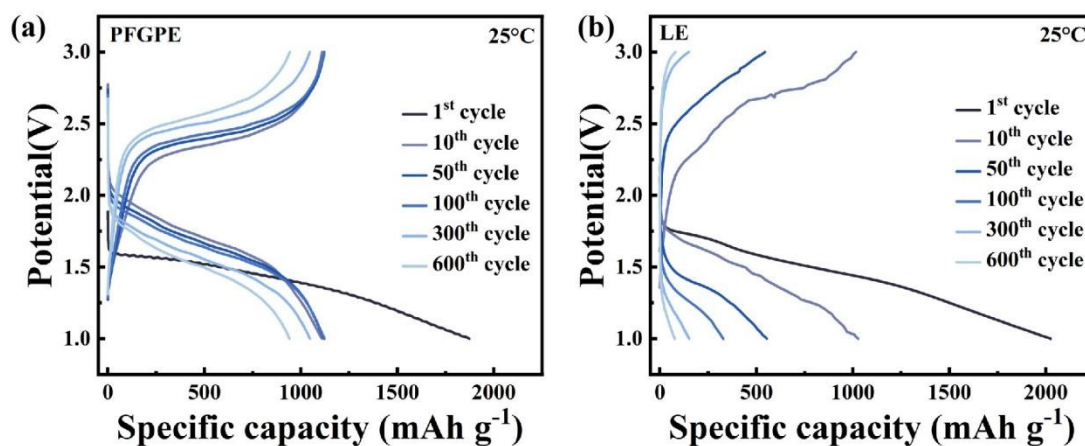


Figure S26. Galvanostatic charge/discharge profiles of ester-based (a) SPAN/PFGPE/Li and (b) SPAN/LE/Li battery at 0.5C and 25 °C.

Table S1. Binding energy and peak assignment of C 1s.

Binding energy (eV)	Peak assignment
284.8	C-C, C=C
285.7-286.3	C-N, C-O
288.4-288.9	C=O, O-C=O
289.9-291	Li ₂ CO ₃ , C-F from PVDF
292.8-293.3	CF ₃

Table S2. Binding energy and peak assignment of O 1s.

Binding energy (eV)	Peak assignment
530.7-532.1	C=O, O-C=O, Li ₂ CO ₃
532.3-533.2	C-O

Table S3. Binding energy and peak assignment of S 2p

Binding energy (eV)	Peak assignment
160-162.6	Li ₂ S
161.7-163.2	Li ₂ S ₂
163-164.6	bridging S
164.5-165	S
166.1-168	thiosulfate
168.6-172	poly-thionate

Table S4. Binding energy and peak assignment of F 1s.

Binding energy (eV)	Peak assignment
684.6-685	LiF
687.6	C-F · PVDF

Table S5. Cycle performance of ester-based Li-SPAN batteries.

Active material	Electrolyte	Reversible discharge capacity (mAh g ⁻¹)	Capacity (mAh g ⁻¹)	Capacity retention	Rate	Cycles	Ref.
SPAN	PFGPE	1392.68	1324.24	95.1%	0.1C/25 °C	200	This work
		1128.4	945.2	83.8%	0.5C/25 °C	600	
		878.37	624.9	71.1%	1C/25 °C	900	
SPAN	PVDF-HFP/ PMMA/ MMT	1,108	1095.8	98.8%	0.1C/25 °C	100	[8]
SPAN	PVDF- HFP/LiFSI	1324.96	897.4	67.7%	0.2C/25 °C	100	[9]
SPAN	PVDF-HFP/ PMMA/ MPS	1340	1143	85.2%	0.2C/25 °C	100	[10]
SPAN	LCE	1300	588	45.2%	0.1C/60 °C	50	[11]
SPAN	Poly-S electrolyte	989.07	905	91.5%	0.1C/25 °C	100	[12]
SPAN	ACA/BP-Li	1289.56	938	72.73%	0.5C/25 °C	500	[13]
SPAN	FRSPE	1311.3	944.13	72%	0.5C/25 °C	100	[14]

References

- [1] G. Kresse, J. Hafner, Ab, *Phys. Rev. B.*, 1993, **47**, 558–561.
- [2] G. Kresse, J. Hafner, Ab, *Phys. Rev. B.*, 1994, **49**, 14251–14269.
- [3] J. P. Perdew, K. Burke, M. *Phys. Rev. Lett.*, 1996, **77**, 3865–3868.
- [4] G. Kresse, D. Joubert, *Phys. Rev. B.*, 1999, **59**, 1758–1775.
- [5] P. E. Blöchl, P. A.W. Method, *Phys. Rev. B.*, 1994, **50**, 17953–17979.
- [6] K. Yan, J. Wang, S. Zhao, D. Zhou, B. Sun, Y. Cui, G. Wang, *Angew. Chem. Int. Ed.*, 2019, **58**, 11364–11368.
- [7] X. Chen, X. Chen, T. Hou, B. Li, X. Cheng, R. Zhang, Q. Zhang, *Sci. Adv.*, 2019, **5**, eaau7728.
- [8] Y. Zhang, Y. Zhao, Z. Bakenov, D. Gosselink, P. Chen, *J Solid State Electrochem.*, 2014, **18**, 1111–1116.
- [9] C. Li, Q. Zhang, J. Sheng, B. Chen, R. Gao, Z. Piao, X. Zhong, Z. Han, Y. Zhu, J. Wang, G. Zhou, H. Cheng, *Energy Environ. Sci.*, 2022, **15**, 4289–4300.
- [10] K. Jeddi, M. Ghaznavi, P. Chen, *J. Mater. Chem. A.*, 2013, **1**, 2769.
- [11] M. Li, J. E. Frerichs, M. Kolek, W. Sun, D. Zhou, C. Huang, B. J. Hwang, M. R. Hansen, M. Winter, P. Bieker, *Adv. Funct. Mater.*, 2020, **30**, 1910123.
- [12] Y. Sun, G. Zhong, Z. Zhao, M. Cao, H. Zhou, S. Zhang, H. Qian, Z. Lin, D. Lu, J. Wu, H. Chen, *Nano Lett.*, 2020, **20**, 2191–2196.
- [13] Y. Huang, Y. Wang, Y. Fu, *Carbohydr. Polym.*, 2022, **296**, 119950.
- [14] H. Li, Y. Kuai, J. Yang, S. I. Hirano, Y. N. Nuli, J. Wang, *J. Energy Chem.*, 2022, **65**, 616–622.